Au atom site with a K^+–K^+ distance of 8.22 Å. Since an AuCN molecule should be about 3.3 Å in length, the AuCN molecule could occupy the missing Au atom site and, because of its small size in comparison with the distance between neighbors, have a random orientation with a resulting zero *P* value. In contrast, the powder 430-nm emission band is assigned to emission of $Au(CN)_2^-$ occupying a surface site. This band does not shift in energy with changing temperature, but its relative intensity, in comparison with that of the 390-nm band, can be increased by heating the sample. This is similar to the behavior reported for surface states of metal oxide powder samples.[17,18]

In order to characterize the dynamics of energy transfer between the states that give rise to the 390- and 630-nm bands, measurements have been made of the relative intensities of these bands as a function of temperature. As the temperature of a $KAu(CN)_2$ crystal increases from 80 to 300 K, the relative intensity of the 390-nm band decreases as shown in Figure 5. In contrast, as the temperature of a $KAu(CN)_2$ crystal is increased from 120 to 300 K, the 630-nm band intensity reaches a maximum between 160 and 180 K and then gradually decreases. Similar behavior has been reported for Er^{3+}-doped samples of $CsMnCl_3$ or $RbMnCl_3$.[19]

We interpret the initial increase in the 630-nm intensity from 120 to 160–180 K as arising from increased migration of the 390-nm excitation. A plot of $\log I_{630}$ vs. $1/T$ for ($80 < T < 180$ K) gives an activation energy of 140 cm^{-1}. On the other hand, the decrease of the 630-nm band intensity is probably due to the increasing tendency toward multiphonon relaxation to the ground electronic state of $KAu(CN)_2$ because the CN vibration energy is 2160 cm^{-1}.

Conclusions

The luminescence behavior of the layered compound $KAu(CN)_2$ can be described by a bonding model in which the Au–Au orbitals overlap. A plot of the energy of the high-energy emission band vs. R^{-3}_{Au-Au} confirms that Frenkel exciton behavior exists as in one-dimensional solids. Vibronic structure for the high-energy band is assigned to a CN symmetric stretch mode progression.

A low-energy emission band exists in pure $KAu(CN)_2$ that is assigned to a chemical trap. However, when $Au(CN)_2^-$ is doped into potassium cyanide crystals, the low-energy band does not appear but the high-energy band appears at 78 K with vibronic structure shifted slightly to lower energy compared with that of $KAu(CN)_2$. This implies that clusters of $Au(CN)_2^-$ exist in KCN without light-emitting traps.

Registry No. $KAu(CN)_2$, 13967-50-5.

(17) Anpo, M.; Kubokawa, Y. *J. Phys. Chem.* **1984**, *88*, 5556.
(18) Coluccia, S.; Tench, A. J. *J. Chem. Soc., Faraday Trans. 1* **1983**, *79*, 1881.
(19) Kambli, U.; Gudel, H. U. *Inorg. Chem.* **1984**, *23*, 3479.

Contribution from the Lehrstuhl für Anorganische Chemie I, Ruhr-Universität, D-4630 Bochum, FRG, Fachbereich Chemie, Philipps-Universität, D-3550 Marburg, FRG, Anorganisch-Chemisches Institut der Universität, D-6900 Heidelberg, FRG, and Department of Chemistry, State University of Leiden, 2300 RA Leiden, The Netherlands

Variable-Temperature Single-Crystal Electron Spin Resonance Study and Crystal Structure of $[Cu(C_6H_{15}N_3)_2][Cu(CN)_3]\cdot 2H_2O$ at 110 and 293 K. Static and Dynamic Jahn–Teller Distortions in the CuN_6 Polyhedron

Phalguni Chaudhuri,[1a] Karen Oder,[1a] Karl Wieghardt,*[1a] Johannes Weiss,[1b] Jan Reedijk,[1c] Winfried Hinrichs,[1c] John Wood,*[1c,d] Andrej Ozarowski,[1e] Horst Stratemaier,[1e] and Dirk Reinen*[1e]

Received February 20, 1986

The reaction of $CuCl_2\cdot 2H_2O$ in aqueous solution containing 1,4,7-triazacyclononane ([9]aneN$_3$, $C_6H_{15}N_3$) and KCN afforded blue crystals of $[Cu([9]aneN_3)_2][Cu(CN)_3]\cdot 2H_2O$, the crystal structure of which has been determined at 110 and 293 K. The complex crystallizes in the monoclinic crystal system, space group $P2_1/n$. Crystal data at 110 K and (in brackets) at 293 K: a = 13.119 (2) Å [13.061 (3) Å], b = 12.116 (2) Å [12.380 (3) Å], c = 13.452 (2) Å [13.503 (4) Å], β = 93.90 (2)° [93.06 (2)°] and Z = 4. The structures were refined to conventional R values of 0.024 [0.045] by using 2881 [3547] unique reflections. The compound consists of $[Cu([9]aneN_3)_2]^{2+}$ cations, $[Cu(CN)_3]^{2-}$ anions, and water of crystallization. The geometry of the CuN_6 core is a tetragonally elongated octahedron. At 110 K a maximum Jahn–Teller distortion is displayed with two long axial Cu–N bonds (2.305 (2) and 2.336 (2) Å) and four shorter equatorial Cu–N distances (average 2.062 Å), whereas at 293 K a dynamic component is obviously involved; the two axial Cu–N distances are at 2.222 (3) and 2.234 (3) Å and the average equatorial Cu–N distance is at 2.111 Å. The anion $[Cu(CN)_3]^{2-}$ is trigonal planar; the Cu–C and C–N bond lengths (average 1.934 and 1.135 Å, respectively) do not vary significantly between 110 and 293 K. Single-crystal and powder EPR spectra have been recorded at various temperatures (4.2–340 K), and a model for the dynamic averaging process within the CuN_6 polyhedra is proposed. An analysis of the thermal motion ellipsoids has been attempted with only limited success in order to further characterize the partial dynamic character of the CuN_6 core at 293 K.

Introduction

The small macrocyclic N donor 1,4,7-triazacyclononane ([9]aneN$_3$) is a strong ligand that forms very stable octahedral or distorted-octahedral bis complexes with many divalent and trivalent metal cations of the first transition-metal series.

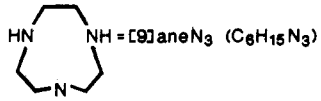

NH = [9]aneN$_3$ ($C_6H_{15}N_3$)

A series of these complexes have been thoroughly studied by spectroscopy (electronic spectra, EPR spectra) and X-ray crystallography, i.e. bis complexes of Cr^{3+},[2] Mn^{2+},[2] Fe^{2+},[2,3] Fe^{3+},[2,3] Co^{2+},[2,4] Co^{3+},[5,6] Ni^{2+},[7,9] and Ni^{3+}.[2,10,11] Their stability toward

(1) (a) Ruhr-Universität Bochum; (b) Universität Heidelberg; (c) State University of Leiden; (d) Visiting professor from the Chemistry Department, University of Massachusetts, Amherst, MA; (e) Philipps-Universität.
(2) Wieghardt, K.; Schmidt, W.; Herrmann, W.; Küppers, H. J. *Inorg. Chem.* **1983**, *22*, 2953–2956.
(3) Boeyens, J. C. A.; Forbes, A. G. S.; Hancock, R. D.; Wieghardt, K. *Inorg. Chem.* **1985**, *24*, 2926–2931.
(4) Kuppers, H. J.; Neves, A.; Pomp, C.; Ventur, D.; Wieghardt, K.; Nuber, B.; Weiss, J. *Inorg. Chem.*, in press.
(5) Koyama, H.; Yoshino, T. *Bull. Chem. Soc. Jpn.* **1972**, *45*, 481–484.
(6) Mikami, W.; Kuroda, R.; Konno, M.; Saito, Y. *Acta Crystallogr., Sect. B: Struct. Crystallogr. Cryst. Chem.* **1977**, *B33*, 1485–1489.
(7) Yang, R.; Zompa, L. J. *Inorg. Chem.* **1976**, *15*, 1499–1502.

0020-1669/86/1325-2951$01.50/0

ligand dissociation in aqueous solution in the divalent and trivalent form of the respective metal centers has shown these complexes to be ideal outer-sphere one-electron oxidants and/or reductants. Their redox potentials were readily measured by cyclic voltammetry,[2] and the electron-transfer self-exchange rate constants of $[M([9]aneN_3)_2]^{3+/2+}$ couples are currently determined[4] and successfully interpreted in the frame of the recently developed semiclassical Marcus–Sutin model[12] for outer-sphere electron-transfer reactions.

Since this ligand is a pure σ-donor, the stereochemistry of MN_6 cores as a function of the electronic configuration of the respective metal center and of its effective ionic radius is readily studied.

One of the most interesting aspects in this respect is the investigation of complexes containing a metal center with an electronic configuration that, in an octahedral ligand field, exhibits static or dynamic Jahn–Teller distortions of the MN_6 core (e.g. high-spin d^4, low-spin d^7 and d^9). We have recently undertaken a careful study of the Jahn–Teller cations $[Ni([9]aneN_3)_2]^{3+}$ [11] and $[Co[9]aneN_3)_2]^{2+}$.[4] We report here our results on $[Cu([9]aneN_3)_2]^{2+}$, which has been prepared in crystalline forms as $[Cu([9]aneN_3)_2][Cu(CN)_3]\cdot 2H_2O$. $[Cu([9]aneN_3)_2]Cl_2\cdot 4.5H_2O$ and $[Cu([9]aneN_3)_2](NO_3)_2$ have been isolated previously.[7] The electronic spectrum in aqueous solution (λ_{max} = 8100 cm^{-1} (ϵ = 48 L mol^{-1} cm^{-1}) and 16 130 cm^{-1} (ϵ = 360 L mol^{-1} cm^{-1})) has been reported. We have determined the crystal structure of $[Cu([9]aneN_3)_2][Cu(CN)_3]\cdot 2H_2O$ at 110 and 293 K and have measured the single-crystal and powder EPR spectra at various temperatures.

Experimental Section

The ligand 1,4,7-triazacyclononane was prepared according to procedures described in the literature.[13]

$[Cu([9]aneN_3)_2][Cu(CN)_3]\cdot 2H_2O$. To an aqueous solution (50 mL) of $CuCl_2\cdot 2H_2O$ (0.34 g, 2 mmol) were added an 1 M ethanolic solution (2 mL) of the ligand 1,4,7-triazacyclononane and an aqueous solution (50 mL) of KCN (0.12 g, 2 mmol) at room temperature. This solution was allowed to stand in an open vessel for 3–4 days, during which time blue crystals of the desired product precipitated, which were filtered off and air-dried (yield: 0.21 g; 23% based on Cu). Anal. Calcd for $C_{15}H_{34}N_9Cu_2O_2$: C, 36.06; H, 6.86; N, 25.23; Cu, 25.44. Found: C, 35.9; H, 6.8; N, 25.1; Cu, 26.0.

Instrumentation. The ligand field reflection spectra were recorded on a Zeiss PMQ II spectrophotometer (Infrasil) with Sr_2ZnTeO_6 [(4–12) $\times 10^3$ cm^{-1}] and freshly sintered MgO [(8–30) $\times 10^3$ cm^{-1}] as standards. The single-crystal and powder EPR spectra (35 GHz) were measured with a Varian E 15 spectrometer at 4.2 and 77 K and—with a Varian variable-temperature accessory—between 130 and 380 K. DPPH was used as internal standard (g = 2.0037).

X-ray Structure Determinations. Precise lattice constants of $[Cu([9]aneN_3)_2][Cu(CN)_3]\cdot 2H_2O$ and diffracted intensities were obtained from measurements carried out at 110 K on an Enraf-Nonius CAD 4 diffractometer and at 293 K on an AED II (Siemens) diffractometer. The setting angles of 24 (110 K) and 30 (293 K) reflections in the range $22 \leq 2\theta \leq 28°$ were determined by using the automatic centering programs supplied with the computer-controlled diffractometers. Crystal cooling was achieved with an N_2-gas stream (110 ± 3 K) produced by a locally modified Enraf-Nonius low-temperature unit. Least-squares refinements of these reflections led to the lattice constants summarized in Table I. Intensity data at 110 K were measured by using the ω/θ step-scan technique, where the scans were analyzed by using the program PROFILE.[14] Three standards were monitored, and a uniform decrease of ca. 7% in intensity from the beginning to the end of data collection was observed, for which corrections were made. At 293 K intensity data were measured by θ–2θ scans; no decay of intensity was observed during data collection. The intensity data were corrected for Lorentz and polarization effects in the usual manner. Absorption corrections have also been carried out by using the Monte Carlo method[15] (110 K) and ψ scans (293 K). The structure was solved via conventional Patterson and Fourier syntheses. In all structure factor calculations the atomic scattering factors used were taken from the ref 16. Anomalous dispersion corrections for Cu were included.[17] The structure was refined by full-matrix least-squares methods,[18] and the quantity minimized was $\sum w(|F_o| - |F_c|)^2$ with weights $w = [2LpF_o/\sigma(I)^2]$ at 110 K and $w = 1/\sigma(F_o)^2$ at 293 K. All non-hydrogen atoms were refined with anisotropic thermal parameters. At 110 K the positions of all hydrogen atoms were located in difference Fourier syntheses and were included in the refinements with isotropic thermal parameters. At 293 K these positions could not be

Table I. Crystallographic Data for $[Cu([9]aneN_3)_2][Cu(CN)_3]\cdot 2H_2O$ at 293 and 110 (3) K

	$[Cu(C_6H_{15}N_3)_2][Cu(CN)_3]\cdot 2H_2O$	
	293 K	110 K
mol wt	499.6	499.6
a, Å	13.061 (3)	13.119 (2)
b, Å	12.380 (3)	12.116 (2)
c, Å	13.503 (4)	13.452 (2)
β, deg	93.06 (2)	93.90 (2)
V, Å^3	2180	2133.4
Z	4	4
space group	$P2_1/n$; $\pm h,k,l$	$P2_1/n$; $\pm h,k,l$
d_{calcd}, g/cm^2	1.522	1.555
cryst dimens, mm^3	0.2 × 0.4 × 0.6	0.26 × 0.15 × 0.20
abs coeff (μ), cm^{-1}	21.6	21.6
transmission factors, max–min	0.68–0.59	0.735–0.68
instrument	AED II Siemens	CAD 4 Enraf-Nonius
radiation (graphite-monochromated)	Mo Kα	Mo Kα
$2\theta_{max}$, deg	60	50
total no. of data	5641	4121
no. of data used in refinement ($I \geq 2.0\sigma(I)$)	3547	2881
no. of atoms	58	58
no. of variables	253	389
R	0.045	0.024
R_w	0.041	0.029
max shift/esd in last cycle	0.03	0.01

[a] λ = 0.710 69 Å.

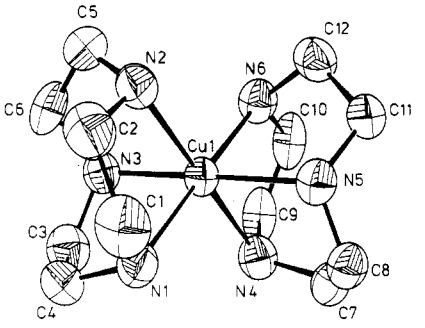

Figure 1. Perspective view of the cation $[Cu([9]aneN_3)_2]^{2+}$ at 293 K and the atomic labeling scheme.

(8) (a) Zompa, L. J. *Inorg. Chem.* **1978**, *17*, 2531–2536. (b) Nonayama, M. *Transition Met. Chem. (Weinheim, Ger.)* **1976**, *1*, 70–74.
(9) Zompa, L. J.; Margulis, T. N. *Inorg. Chim. Acta* **1978**, *28*, L157–L159.
(10) McAuley, A.; Norman, P. R.; Olubuyide, O. *Inorg. Chem.* **1984**, *23*, 1938–1943; *J. Chem. Soc., Dalton Trans.* **1984**, 1501–1505.
(11) Wieghardt, K.; Walz, W.; Nuber, B.; Weiss, J.; Ozarowski, A.; Stratemaier, H.; Reinen, D. *Inorg. Chem.* **1986**, *25*, 1650–1654.
(12) (a) Sutin, N. *Acc. Chem. Res.* **1982**, *15*, 275–282. Sutin, N. *Progr. Inorg. Chem.* **1983**, *30*, 441–498. (b) Brunschwig, B. S.; Creutz, C.; Macartney, D. H.; Sham, T. K.; Sutin, N. *Discuss. Faraday Soc.* **1982**, *74*, 113–127.
(13) (a) Atkins, T. J.; Richman, J. E.; Oettle, W. F. *Org. Synth.* **1978**, *58*, 86–97. (b) Wieghardt, K.; Schmidt, W.; Nuber, B.; Weiss, J. *Chem. Ber.* **1979**, *112*, 2220–2230.
(14) Blessing, R. H.; Coppens, P.; Becker, P. *J. Appl. Crystallogrg.* **1974**, *7*, 488.
(15) de Graaf, R. A. G. *Acta Crystallogr., Sect. A: Cryst. Phys., Diffr., Theor. Gen. Crystallogr.* **1973**, *A29*, 298.
(16) *International Tables for X-ray Crystallography*; Kynoch: Birmingham, England, 1974; Vol. IV, pp 72–98.
(17) Cromer, D. T.; Libermann, D. *J. Chem. Phys.* **1970**, *53*, 1891–1898.
(18) Computations were carried out by using a locally modified version of ORFLS (Busing, W. R.; Martin, K. O.; Levy, H. A. ORFLS, Report ORNL-TM-305; Oak Ridge National Laboratory: Oak Ridge, TN, 1962) for the low-temperature study and the program package STRUCSY (Structure computation system; Stoe, Darmstadt, FRG) for the room-temperature study.

Table II. Atomic Coordinates[a] of $[Cu([9]aneN_3)_2][Cu(CN)_3]\cdot 2H_2O$ at 110 and 293 K

	x/a		*y/b*		*z/c*	
atom	110 K	293 K	110 K	293 K	110 K	293 K
Cu1	24696 (2)	24780 (2)	25358 (2)	24960 (2)	-302 (2)	-290 (2)
Cu2	35823 (2)	34600 (2)	71350 (2)	70700 (2)	12703 (2)	12150 (2)
O1	7743 (2)	7909 (3)	1719 (2)	1822 (3)	1728 (2)	1645 (3)
O2	5485 (2)	5479 (3)	1099 (2)	1087 (4)	2686 (2)	2592 (3)
N1	1318 (2)	1377 (2)	1135 (2)	1159 (2)	192 (2)	184 (2)
N2	2351 (2)	2411 (2)	1932 (2)	1868 (2)	-1456 (2)	-1474 (2)
N3	3460 (2)	3523 (2)	1213 (2)	1204 (2)	229 (2)	227 (2)
N4	2594 (2)	2550 (2)	3182 (2)	3162 (2)	1391 (2)	1420 (2)
N5	1505 (2)	1451 (3)	3858 (2)	3790 (2)	-297 (2)	-289 (2)
N6	3676 (2)	3614 (3)	3922 (2)	3818 (3)	-230 (2)	-228 (2)
N7	1265 (2)	1133 (4)	6935 (2)	6915 (4)	1449 (2)	1344 (3)
N8	5083 (2)	4923 (3)	6584 (2)	6497 (4)	3067 (2)	2986 (3)
N9	4371 (2)	4312 (3)	7832 (2)	7775 (4)	-736 (2)	-745 (3)
C1	777 (2)	851 (3)	1097 (2)	1065 (4)	-800 (2)	-803 (3)
C2	1519 (2)	1578 (3)	1100 (2)	1070 (3)	-1625 (2)	-1618 (3)
C3	1899 (2)	1947 (3)	136 (2)	191 (3)	492 (2)	512 (3)
C4	2981 (2)	3019 (3)	423 (2)	451 (3)	895 (2)	885 (3)
C5	3381 (2)	3442 (3)	1478 (2)	1422 (4)	-1592 (2)	-1581 (3)
C6	3703 (2)	3789 (3)	716 (2)	727 (3)	-740 (2)	-733 (3)
C7	1774 (2)	1729 (3)	4014 (2)	3975 (3)	1513 (2)	1517 (3)
C8	985 (2)	944 (3)	3969 (2)	3912 (3)	643 (2)	656 (3)
C9	3638 (2)	3596 (3)	3630 (2)	3594 (3)	1594 (2)	1597 (3)
C10	3935 (2)	3885 (3)	4393 (2)	4313 (3)	768 (2)	743 (3)
C11	2038 (2)	1984 (4)	4883 (2)	4780 (3)	-583 (2)	-597 (3)
C12	3098 (2)	3054 (4)	4658 (2)	4534 (3)	-925 (2)	-935 (3)
C13	2122 (2)	1988 (4)	7049 (2)	7015 (4)	1373 (2)	1297 (3)
C14	4516 (2)	4389 (4)	6767 (2)	6702 (4)	2395 (2)	2332 (3)
C15	4090 (2)	4015 (3)	7566 (2)	7506 (4)	9 (2)	-21 (4)

[a] Coordinates $\times 10^4$ except for Cu1 and Cu2 where the factor is 10^5.

Table III. Bond Distances (Å) and Angles (deg) in $[Cu([9]aneN_3)_2][Cu(CN)_3]\cdot 2H_2O$ at 110 and (in Brackets) at 293 K

	(a) Coordination Polyhedron		
Cu1–N1	2.305 (2) [2.222 (3)]	Cu1–N6	2.336 (2) [2.234 (3)]
Cu1–N2	2.048 (2) [2.098 (3)]	Cu1–N4	2.063 (2) [2.120 (3)]
Cu1–N3	2.077 (2) [2.119 (3)]	Cu1–N5	2.058 (2) [2.106 (3)]
N1–Cu1–N2	81.4 (1) [81.3 (2)]	N6–Cu1–N4	79.7 (1) [80.2 (2)]
N1–Cu1–N3	79.5 (1) [80.3 (2)]	N6–Cu1–N5	80.4 (1) [81.0 (2)]
N2–Cu1–N3	83.6 (1) [82.3 (2)]	N4–Cu1–N5	82.9 (1) [81.7 (2)]
N1–Cu1–N4	99.8 (1) [99.6 (2)]	N6–Cu1–N2	99.1 (1) [98.9 (2)]
N1–Cu1–N5	101.3 (1) [100.2 (2)]	N6–Cu1–N3	98.8 (1) [98.5 (2)]
N2–Cu1–N5	96.2 (1) [97.6 (2)]	N3–Cu1–N4	97.4 (1) [98.4 (2)]
	(b) Anion		
Cu2–C13	1.933 (3) [1.932 (5)]	C13–N7	1.144 (4) [1.129 (7)]
Cu2–C14	1.933 (3) [1.940 (5)]	C14–N8	1.153 (4) [1.124 (7)]
Cu2–C15	1.937 [1.931 (5)]	C15–N9	1.137 (4) [1.122 (6)]
C13–Cu2–C14	120.7 (1) [122.0 (4)]	Cu2–C13–N7	176.0 (3) [175.9 (7)]
C14–Cu2–C15	120.7 (1) [119.3 (4)]	Cu2–C14–N8	177.8 (3) [178.0 (7)]
C13–Cu2–C15	118.6 (1) [118.7 (4)]	Cu2–C15–N9	178.6 (3) [177.5 (7)]

located, with the exception of hydrogens bound to nitrogen, and the contribution of hydrogen bound to carbon was introduced in calculated positions (C–H = 0.96 Å and sp^3-hybridized carbon atoms, with isotropic thermal motion). The final values of $R = \sum||F_o| - |F_c||/\sum|F_o|$ and $R_w = [\sum w(|F_o| - |F_c|)^2/\sum w|F_o|^2]^{1/2}$ are summarized in Table I. At convergence, final difference Fourier syntheses were essentially featureless with maximum and minimum values being 40% of a peak assigned as hydrogen. The final atomic positional parameters are given in Table II. Listings of observed and calculated structure factors, anisotropic thermal parameters, and positional parameters of hydrogen atoms are available as supplementary material.

Results and Discussion

From an aqueous solution containing $CuCl_2\cdot 2H_2O$ and the ligand 1,4,7-triazacyclononane in equimolar amounts, after addition of a small amount of KCN, bright blue crystals of X-ray quality of the mixed-valence salt $[Cu([9]aneN_3)_2][Cu(CN)_3]\cdot 2H_2O$ precipitated within 2–3 days.

Crystal Structures at 110 and 293 K. Crystals of $[Cu([9]aneN_3)_2][Cu(CN)_3]\cdot 2H_2O$ consist of discrete cations of $[Cu([9]aneN_3)_2]^{2+}$ and the anion $[Cu(CN)_3]^{2-}$ and molecules of water of crystallization. Figures 1 and 2 give a perspective view of the cation and the anion, respectively, showing the anisotropic thermal ellipsoids at 293 K and the respective atomic labeling scheme. Selected bond distances and angles are summarized in Table III.

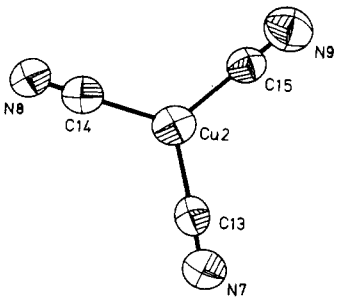

Figure 2. Perspective view of the anion $[Cu(CN)_3]^{2-}$ at 293 K and the atomic labeling scheme.

Between 110 and 293 K the crystals do not undergo a phase transition; only a small decrease of 2.16% of the unit cell volume is observed as the temperature decreases from 293 to 110 K. The

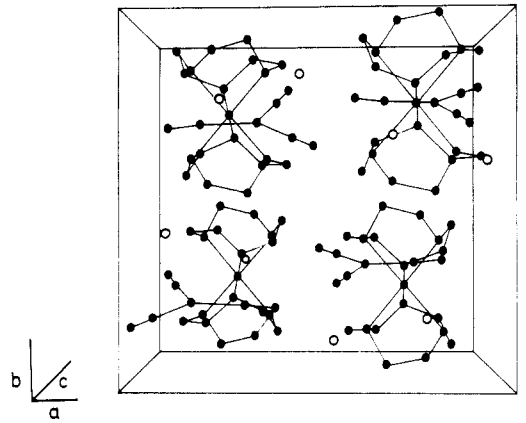

Figure 3. Packing diagram of $[Cu([9]aneN_3)_2][Cu(CN)_3]\cdot 2H_2O$ (open circles denote molecules of water of crystallization).

monomeric anion $[Cu(CN)_3]^{2-}$ is trigonally planar with practically D_{3h} symmetry, which is not crystallographically imposed. The anions are totally ordered in the crystal, contrasting the previously reported structure of $Na_2[Cu(CN)_3]\cdot 3H_2O$.[19] This trigonal coordination of copper(I) in the solid state is quite rare for mononuclear complexes of Cu(I); a further example is found in $[Cu(en)_3][Cu(CN)_3]$,[20] the structure of which has not been determined by X-ray crystallography. Interestingly, the Cu(I)–C and C–N bond lengths of the anion are, within experimental error, identical at 110 and 293 K (Table III). The average Cu–C distance of 1.934 Å and C–N distance of 1.135 Å agree well with those found in $Na_2[Cu(CN)_3]\cdot 3H_2O$.[19] Thus this metrical information of the anion serves ideally as an internal standard for the degree of the observed temperature effect on the structure of the cation $[Cu([9]aneN_3)_2]^{2+}$ (see below).

The tridentate macrocycles are coordinated facially to the copper(II) centers, which show octahedral coordination with differing degrees of distortion (Figure 1). Bond lengths and angles at 110 and 293 K are given in Table III; intraligand C–N and C–C distances, which do not vary with temperature, are available as supplementary material. A perspective view of the crystal packing is shown in Figure 3. Only the amine nitrogen atoms N5 and N2 form relatively strong N–H···O hydrogen bonds to the two molecules of water of crystallization, O2 and O1, respectively (2.942 (4) and 3.013 (4) Å at 110 K, respectively). Two additional, rather weak hydrogen-bonding interactions between the amine nitrogens N1 and N3 and the nitrogens N8 and N9 of the complex anion at distances of 3.121 (3) and 3.105 Å, respectively, are observed. All three terminal nitrogens of the anion $[Cu(CN)_3]^{2-}$ form strong hydrogen bonds to the oxygens of the molecules of water of crystallization (O2···N7, 2.830 (3) Å; O1···N8, 2.851 Å; O2···N9, 2.944 (3) Å at 110 K).

The CuN_6 chromophore of the cation $[Cu([9]aneN_3)_2]^{2+}$ involves an elongated rhombic octahedral stereochemistry, but with significant differences in the Cu–N bond lengths at 110 and 293 K (Table III), which result in a clear difference in the resulting tetragonalities, T, of 0.885 at 110 K and 0.947 at 293 K (where T is the mean in-plane Cu–N bond length divided by the mean out-of-plane Cu–N bond length[21]). It is noted that due to the steric constraints of the nine-membered ring of the ligands a trigonal distortion of the CuN_6 polyhedron is also apparent. The N–Cu–N bond angles within each coordinated triamine are significantly smaller than 90° (average ~81°) whereas N–Cu–N angles of nitrogen atoms in cis position of different ligands are >90° (average 98.5°).

In the crystal structure of $(NH_4)_2[Cu(OH_2)_6](SO_4)_2$ at room and liquid-nitrogen temperatures the CuO_6 core also becomes more elongated and axial with decreasing temperature (T = 0.914 at room temperature and 0.864 at 150 K).[22] In $[Cu\{HB(N_2C_3H_3)_3\}_2]$ containing two tripoidal hydrotris(pyrazolyl-1-yl)borato ligands the interesting situation is encountered where two independent molecules with differing degrees of tetragonalities (T = 0.792 and 0.866) are in the unit cell (distortion isomers)[23] at room temperature. In two different salts containing the cation $[Cu(tach)_2]^{2+}$, namely $[Cu(tach)_2](NO_3)_2$ and $[Cu(tach)_2](ClO_4)_2$, where tach is *cis,cis*-1,3,5-triaminocyclohexane, the former displays a tetragonality of 1.0 and the latter of 0.88 at room temperature.[24]

The variations in the Cu–N distances between 110 and 293 K are indicative of a dynamic Jahn–Teller process in which one well in the warped "Mexican hat" potential energy surface[28] is more stable than the other two. Despite the lack of any crystallographic site symmetry for the $[Cu([9]aneN_3)_2]^{2+}$ ion, the nearly identical average Cu–N bond lengths at 293 and 110 K (2.150 and 2.148 Å, respectively) are fully in accord with such a process and the differences between centrosymmetrically related bonds and the departure from tetragonal geometry for the CuN_6 moiety can presumably be attributed to the differing environments of ligands 1 and 2 (1, atoms N1, N2, and N3; 2, atoms N4, N5, and N6).

Table IV. Root-Mean-Square Displacements (Å) of the Nitrogen Atoms along Their Thermal Ellipsoid Principal Axes and the Angles (α, deg) of These Axes with the Cu–Ni (i = 1–6) Vectors

	295 K		110 K	
atom	$(U_{ii})^{1/2}$	α	$(U_{ii})^{1/2}$	α
N1	0.204	87.1	0.103	74.7
	0.229	10.6	0.138	17.1
	0.248	79.8	0.159	97.4
N2	0.197	103.6	0.106	79.0
	0.220	20.2	0.125	11.8
	0.253	104.6	0.161	85.8
N3	0.202	104.3	0.122	98.1
	0.225	67.4	0.130	89.2
	0.231	27.2	0.145	8.2
N4	0.183	87.1	0.086	74.6
	0.209	13.5	0.128	16.3
	0.248	76.9	0.171	95.4
N5	0.189	76.4	0.110	80.6
	0.210	22.4	0.140	24.8
	0.290	72.5	0.185	67.3
N6	0.208	106.3	0.132	29.0
	0.228	126.0	0.134	88.7
	0.273	40.6	0.178	61.1

Table V. Differences between Mean-Square Displacements of Copper and Nitrogen Atoms along the Appropriate Cu–N Bond Vectors

	ΔU_{CuN}[a]	
atom	295 K	110 K
N1	0.0152	0.0035
N2	0.0176	0.0056
N3	0.0164	0.0075
N4	0.0133	0.0060
N5	0.0114	0.0080
N6	0.0267	0.0054

[a] $\Delta U_{CuN} = U_{Ni} - U_{Cu}$.

(19) Kappenstein, C.; Hugel, R. P. *Inorg. Chem.* **1978**, *17*, 1945–1949.
(20) Wicholas, M.; Wolford, T. *Inorg. Nucl. Chem. Lett.* **1975**, *11*, 157–159.
(21) Hathaway, B. J.; Hodgson, P. G. *J. Inorg. Nucl. Chem.* **1973**, *35*, 4071–4081.
(22) (a) Duggan, M.; Murphy, A.; Hathaway, B. J. *Inorg. Nucl. Chem. Lett.* **1979**, *15*, 103–108. (b) van der Zee, J. J.; Shields, K. G.; Graham, A. J.; Kennard, C. H. L. *Cryst. Struct. Commun.* **1972**, *1*, 367–369. (c) Shields, K. G.; Kennard, C. H. L. *Cryst. Struct. Commun.* **1972**, *1*, 189–191.
(23) Murphy, A.; Hathaway, B. J.; King. T. J. *J. Chem. Soc., Dalton Trans.* **1979**, 1646–1650.
(24) Ammeter, J. H.; Bürgi, H. B.; Gamp, E.; Meyer-Sanderin, V.; Jensen, W. P. *Inorg. Chem.* **1979**, *18*, 733–750.
(25) Cullen, D. L.; Lingafelter, E. C. *Inorg. Chem.* **1970**, *9*, 1858–1864.
(26) Wood, J. S.; Keijzers, C. P.; de Boer, E.; Buttafavâ, A. *Inorg. Chem.* **1980**, *19*, 2213–2225.
(27) Schomaker, V.; Trueblood, K. N. *Acta Crystallogr., Sect. B: Struct. Crystallogr. Cryst. Chem.* **1968**, *B24*, 63–76.
(28) Reinen, D.; Friebel, C. *Struct. Bonding (Berlin)* **1979**, *37*, 1–60.

Table VI. Rigid-Body Parameters for $[Cu([9]aneN_3)_2]^{2+}$ in an Inertial Axis System[a]

	110 K				295 K		
	x	*y*	*z*		*x*	*y*	*z*
			(1) Amplitudes of Libration (deg)				
L_1 = 3.27	101.5	94.6	12.4	L_1 = 4.90	101.5	97.4	13.7
L_2 = 1.76	30.9	62.2	77.7	L_2 = 3.18	25.4	68.9	76.5
L_3 = 1.28	118.3	28.2	91.5	L_3 = 2.32	112.3	22.4	87.7
			(2) Translational Amplitudes (Å)				
T_1 = 0.141	123.6	33.8	86.4	T_1 = 0.216	115.3	27.5	79.8
T_2 = 0.116	92.3	95.9	6.3	T_2 = 0.202	99.0	105.3	17.9
T_3 = 0.108	33.7	56.9	84.8	T_3 = 0.185	27.1	67.7	75.5

[a] Defined as *x* parallel to the N_4–N_5 vector and *z* parallel to the pseudo-3-fold axis of the ligands.

Table VII. Root-Mean-Square Deviations (Å²)[a] between Observed and Calculated Thermal Motion Parameters for Rigid-Body Models

	rms deviation			
	295 K	110 K	N_o[b]	N_v
ligand 1	0.0050	0.0016	54	20
ligand 2	0.0037	0.0021	54	20
complex	0.0051	0.0019	114	20
av $\sigma(U_{obsd})$	0.0023	0.0012		

[a] Defined as $[\sum_{obsd} w(U_{obsd} - U_{calcd})^2/(N_o - N_v)]^{1/2}$. [b] N_o = number of observations; N_v = number of variables.

It seems likely that the hydrogen-bonding contacts are at least partially responsible for this, all three nitrogen atoms of ligand 1 being involved in such interactions, while only N5 of Ligand 2 is involved.

On the basis of experience,[24,25] one might anticipate that the partial dynamic character of the room-temperature structure would also be reflected in the thermal motion ellipsoids. We have accordingly made a comparison of the room- and low-temperature thermal parameters, and these results are collected in Tables IV and V for the CuN_6 moiety and in Tables VI and VII for the entire complex cation. Table IV gives the principal rms components and their angles with respect to the appropriate copper–nitrogen bond vectors, while Table V gives the difference between components along the bond vectors. As can be seen from Table IV there is relatively little change in the orientation angles for the ellipsoid principal axes on going from 295 to 110 K, apart possibly from those for N6. Although for the dynamic regime the largest components of the tensors are normally oriented along or close to the bond vectors,[24,26] this is only true in the present example for atom N3 and, in any event, this orientation is also found at 110 K. In a similar fashion, the dynamic behavior is also usually manifested in the difference between the mean-square displacements, ΔU_{CuN}, along the bond directions. For Jahn–Teller inactive systems, the ΔU values would be anticipated to be rather small, corresponding only to the contribution of the usual stretching motions of fairly rigid bonds, and comparison of related Ni(II) and Cu(II) complexes shows that the major contribution to the *U* values for the latter arises from the dynamic distortion.[24] Examination of the results in Table V indicates that, as might be anticipated, the room-temperature ΔU values are somewhat smaller than those observed for the fully dynamic situation, apart from those for atom N6 but that the differences at 110 K are rather larger than would be expected for a single statically distorted complex. The largest changes occur for atoms N1 and N6, which is as might be expected since these are the bonds that show the largest change in length.

The overall conclusion is that the thermal ellipsoid data for the CuN_6 moiety alone do not permit a straightforward quantitative assessment of the Jahn–Teller parameters for the $[Cu([9]aneN_3)_2]^{2+}$ complex, presumably because even though the room-temperature structure is partially dynamic, the contributions from the complexes in the upper wells are apparently not large enough to cause major changes in ellipsoid orientation in going from 295 to 110 K.

In addition to the foregoing analysis we have carried out a rigid-body analysis[27] of the complete complex cation and the individual ligands, and the results for the former are given in Table VI. The largest libration amplitude for both the complex and the ligands is almost parallel to the pseudo threefold axis of the complex, as is found for the ligand in the $[M(tach)_2]^{2+}$ complexes,[24] and the **T** and **L** tensors are nearly aligned. However, as seen from a comparison of the root-mean-square deviations derived from the least-squares fitting with the averaged $\sigma(U_{obsd})$ values given in Table VII, the quality of the agreement between the observed *U* values and those calculated from the **T**, **L**, and **S** tensors is rather poor for both the ligands individually and the complete complex and suggest that the rigid-body model is a rather poor approximation in the present instance and especially so for the 295 K data. This situation is in marked contrast to the results obtained for the $[Cu(tach)_2]^{2+}$ complexes,[24] where a detailed analysis of the motion of the rigid tach ligand relative to the copper atom was possible and led to a meaningful estimate of the Jahn–Teller parameters. Such an analysis does not appear possible for the $[Cu([9]aneN_3)_2]^{2+}$ complex in view of the nonrigid behavior of the ligands, and we suspect that the molecular motion in the crystal is complicated by the low site symmetry of the complex and the associated asymmetric hydrogen-bonding pattern.

Distortion of the "CuN_6" Polyhedra in $[Cu([9]aneN_3)_2][Cu(CN)_3]\cdot 2H_2O$. Temperature-Dependent Spectroscopic Measurements. The ligand field reflection spectra at 298 K are indicative of a pseudotetragonal symmetry caused by the Jahn–Teller effect. We detected a weak and broad band at 7200 cm^{-1}, which should be due to the transition between the split levels of the octahedral, σ-antibonding ^2E ground state, and a stronger, nearly symmetric band at 16 300 cm^{-1}. The latter corresponds to the transition to the octahedral $^2T_2$ level, whose orbital degeneracy is obviously not lifted within the experimental bandwidth. This is expected, because the $^2T_2$ state is π-antibonding and 1,4,7-triazacyclononane is a pure σ-donor ligand. The splitting of the E ground state is only slightly lower than the one for $[Cu(NO_2)_6]^{4-}$ complexes ($4E_\pi$ = 8000 ± 800 cm^{-1}),[28] and—remembering that the NO_2^- and "[9]ane" ligands are rather similar with respect to their d-bonding properties[29]—one might expect a similar distortion of the CuN_6 polyhedra. The radial distortion parameter $\zeta = \{\sum_i 2(\Delta i)^2\}^{1/2}$ (i = x, y, z; i = deviations of the metal–ligand spacings from the average bond length) for the nitro complexes is 0.30 ± 0.05 Å,[28] in very good agreement with the structural data of the complex under discussion at 110 K where ζ = 0.30 Å. It will be demonstrated by the EPR results presented below, that the structural data at 293 K, which imply $\zeta = 0.13_5$ Å, are not those characteristic for the static limit of the distorted polyhedron but that a transition from a dynamic to a static distortion extends over a broad temperture range. The low-temperature structure determination, which was actually performed to check this interpretation by an independent method, confirms the EPR results. Obviously a dynamic component is involved in the distortion of the CuN_6 entity at 293 K.

The hypothetical octahedral ligand field parameter, calculated from the band positions, is $\Delta \simeq 12\,700$ cm^{-1}. This compares well with the Ni^{2+} value[9,29] and confirms our band assignment. The structurally observed distortion of the Cu^{2+} polyhedra is the ex-

(29) Wieghardt, K.; Ozarowski, A.; Reinen, D., submitted for publication.

Table VIII. Single-Crystal and Powder g Values (35 GHz) at Various Temperatures[a]

T, K	g_1^{ex}	g_2^{ex}	g_3^{ex}	$\bar{g}$
4.2	2.18_1	2.10_8	2.05_3	2.11_4
77	2.17_7	2.10_9	2.05_5	2.11_4
145	2.17_5	2.10_9	2.05_9	2.11_4
205	2.16_5	2.10_9	2.06_7	2.11_4
275	2.15_2	2.10_9	2.09_0	2.11_7
340		$\simeq 2.11_7$[b]		

[a] Measured values are equal within the experimental uncertainty $\delta_g = \pm 0.002$. [b] Nearly isotropic signal, $\Delta H_{pp} \simeq 300$ G.

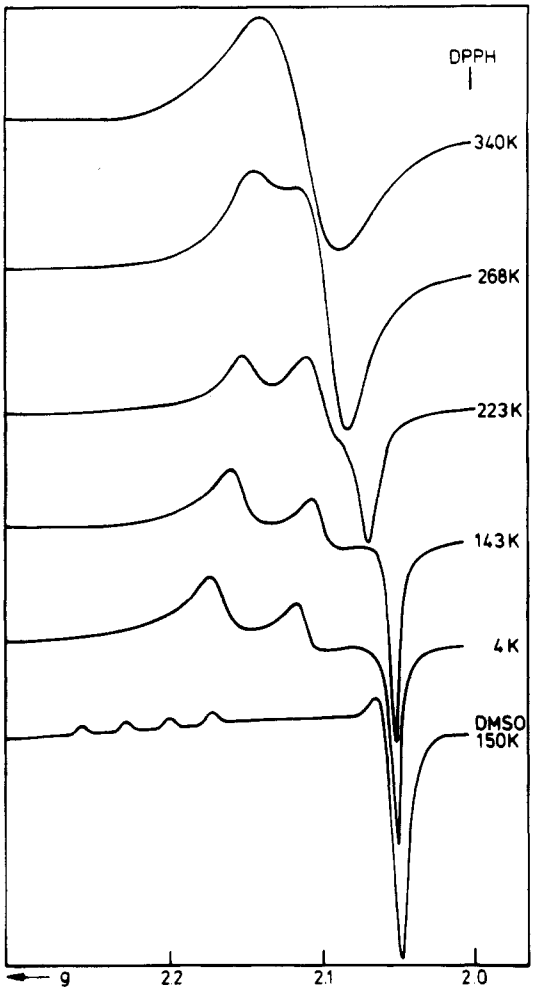

Figure 4. Powder EPR spectra of $[Cu([9]aneN_3)_2][Cu(CN)_3]\cdot 2H_2O$ at various temperatures and frozen-solution EPR spectrum (35 GHz in $(Me_2SO$ at 190 K).

pected tetragonal elongation. This is certainly the result of a vibronic Jahn–Teller coupling, as already anticipated, because the corresponding Ni^{2+} complex has six practically identical Ni–N bond lengths.[9] In both polyhedra the $N–M^{II}–N$ ($M = Ni^{2+}, Cu^{2+}$) bond angles deviate significantly from 90°, however, which is a steric ligand effect of pseudotrigonal symmetry, as already mentioned above.

The temperature dependence of the g values, as obtained from EPR powder spectra, are shown in Figures 4 and 5 and Table VIII. Above ≈120 K the orthorhombic **g** tensor exhibits motional narrowing, without collapsing to a single g value before ~340 K, however. Our working hypothesis is that a transition from a static to the dynamic Jahn–Teller effect is responsible for this behavior, starting at about 120 K and extending over a temperature range of more than 200 K. The situation is rather complicated because the low-temperature **g** tensor (77 K, 4.2 K—Figure 4, Table VIII) with the components $g_1^{ex} = 2.17_9$, $g_2^{ex} = 2.10_9$, and $g_3^{ex} = 2.05_4$ is exchange-coupled. This is deduced from the single-crystal results (see below) and from the frozen-solution

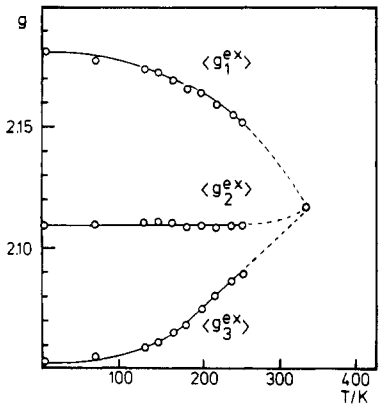

Figure 5. Temperature dependence of the (exchange-coupled) g values of $[Cu([9]aneN_3)_2][Cu(CN)_3]\cdot 2H_2O$.

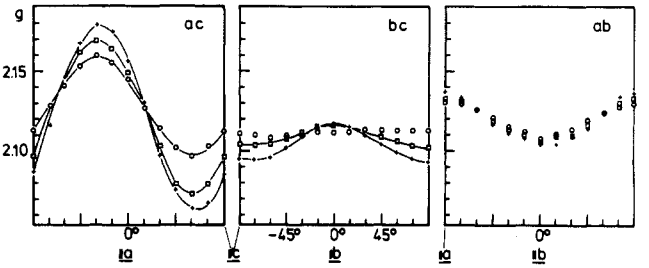

Figure 6. Angular dependence of the EPR signal at 143 (+), 203 (□), and 278 K (○).

spectra in DMF and Me_2SO (Figure 4), which are axial within the error limit and yield quite different g components, namely $g_\parallel = 2.22_9$ and $g_\perp = 2.05_5$. Because the average g values are practically identical, we may assume that the $[Cu([9]aneN_3)_2]^{2+}$ polyhedron remains unchanged in solution and the measured **g** tensor refers to the molecular entity. This is also confirmed by the well-resolved hyperfine structure in the $g_\parallel$ signal ($|A_\parallel| = 177 \times 10^{-4}$ cm^{-1}, Figure 4).

The single-crystal EPR spectra show only one signal, though two magnetically inequivalent Cu^{2+} polyhedra are present in the unit cell. Hence the observed **g** tensor is exchange-coupled. The g components, which are obtained from the angular dependencies of the EPR signal in the *ac*, *bc*, and *ab* planes at 130 K (Figure 6—the deviation of the crystallographic β angle from 90° (~4°) is well within the experimental uncertainty range of the orientation of the single crystal in the magnetic field and is not taken into account) agree with those derived from the powder spectra. While g_2^{ex} correlates with the b axis, g_1^{ex} and g_3^{ex} are located in the *ac* plane with angles of about 115 and 25° with respect to the a axis, respectively (Figure 6). The following model, which is consistent with all available spectroscopic and structural data, is used to translate the exchange-coupled values into the molecular g values. First, it is assumed, that the molecular **g** tensor is axial within the experimental error limit. This is in accord with the structural data, which show four nearly identical short Cu–Ni spacings ($i = 2, 3, 4, 5$) in the CuN_6 polyhedron, and with the frozen-solution EPR spectrum (Figure 4). We further anticipate as a reasonable assumption that the molecular $g_\perp$ value is located in the plane of the these four short bond lengths. Hence $g_\parallel$ should be associated with the normal to this plane—whose direction deviates from the ones of the long Cu–N(6) spacings by about 10°. The thus defined $g_\parallel$ directions of the two magnetically inequivalent CuN_6 polyhedra are inclined with an angle of $\gamma = 55.5°$ to the b axis. Their projections into the *ac* plane have opposite directions, with angles of 17 and 163° with respect to the a axis and 111 and 69° with respect to the c axis. Exchange coupling between the two molecular **g** tensors now induce the following cooperative g values:[30,31]

$$g_1^{ex} = (\sin^2\gamma)g_\parallel + (\cos^2\gamma)g_\perp$$
$$g_2^{ex} = (\cos^2\gamma)g_\parallel + (\sin^2\gamma)g_\perp \qquad g_3^{ex} = g_\perp \tag{1}$$

If one calculates the molecular g values $g_\parallel$ and $g_\perp$ and the angle γ from the observed low-temperature g_1^{ex}, g_2^{ex}, and g_3^{ex} components, one reproduces the frozen-solution g values (Figure 4) and the crystallographic γ angle of $55.5°$ within $\delta g = 0.00_2$ and $\delta_\gamma = 1°$. g_3^{ex} is equivalent to the molecular $g_\perp$ component and should be found in a direction that makes angles of 21 and 73° with respect to the a and c axes, respectively, in reasonable agreement with the experiment (Figure 6).

Because the tridentate ligands are pure σ-donors, the orbital contributions u to the molecular g values are expected to be isotropic. Hence the molecular **g** tensor (static limit at $T \lesssim 120$ K) should obey the relations[28]

$$g_\parallel = g_0 + 8u - 7u^2 \qquad g_\perp = g_0 + 2u - 4u^2 \tag{2}$$

With $u = 0.029$ the frozen solution molecular $g_\parallel$ and $g_\perp$ values can indeed be nicely reproduced. The orbital contributions are defined by

$$u = \frac{k^2\lambda_0}{\Delta E(\rightarrow T_2)}$$

With $g_0 = 2.00_2$, the free-ion LS-coupling parameter $\lambda_0 = 830$ cm^{-1} and the energy of the second band in the ligand field spectrum ($\Delta E = 16\,300$ cm^{-1}), the covalency parameter k is calculated to be 0.75_5. This value is slightly lower than the ones that are characteristic for Cu(II)–nitro complexes ($k \simeq 0.79 \pm 0.02$).[28]

From the observed hyperfine splitting in the $g_\parallel$ signal of the frozen-solution spectra (Figure 4) the mixing coefficient α for the $d_{x^2-y^2}$ orbital in the ground-state MO can be calculated by using the equation

$$A_\parallel = P\left[\left(-\kappa - \frac{4}{7}\right)\alpha^2 + \frac{62}{7}u\right] \tag{3}$$

With the literature values $P = 0.036$ cm^{-1} and $\kappa = 0.43$ and a negative sign for $A_\parallel$,[32] one obtains $\alpha = 0.86_5$, the same value as for Cu^{2+} in nitro complexes.[32] From the corresponding equation for $A_\perp$, a hyperfine splitting constant of -22×10^{-4} cm^{-1} is estimated, which is not resolved in the frozen-solution spectrum, however (Figure 4). In case of a motionally narrowed spectrum (dynamic Jahn–Teller effect) a hyperfine splitting $\bar{A} = {}^1/_3(A_\parallel + 2A_\perp) = -74 \times 10^{-4}$ cm^{-1} is then expected—in excellent agreement with the splitting in the isotropic signal, which is observed in liquid Me_2SO at 298 K ($|\bar{A}| \simeq 75 \times 10^{-4}$ cm^{-1}).

After the discussion of the low-temperature EPR data we will now rationalize the EPR results above 120 K in terms of a continuous transition from a static to a dynamic Jahn–Teller distortion of the CuN_6 polyhedra. We have studied the temperature dependence of EPR powder spectra (Figure 4) as well as the single-crystal spectra at various temperatures (Figure 6), which do not show any significant change in the orientation of g_1^{ex}, g_2^{ex}, and g_3^{ex} with increasing temperature. The g_3^{ex} value is directly indicative of the dynamic fluctuation of $g_\parallel$ between the three (nearly) equivalent orientations perpendicular to the planes of four Cu–Ni spacings, namely with $i = 2$, 3, 4, and 5, $i = 1$, 2, 4, and 6, and $i = 1$, 3, 5, and 6, respectively. We define the probability for $g_\parallel$ to have the direction of the normal to the plane with $i = 2$, 3, 4, and 5 as A and the probability for switching into one of the two alternative directions as B ($A + 2B = 1$). Then the partly or completely dynamically averaged values for $g_3^{ex} = g_\perp$ and $g_\parallel$ at temperatures higher than 120 K are

$$\langle g_\parallel \rangle = g_\parallel - 2B(g_\parallel - g_\perp)$$
$$\langle g_3^{ex} \rangle = \langle g_\perp \rangle = g_\perp + B(g_\parallel - g_\perp) \tag{4}$$

where $g_\parallel$ and $g_\perp$ are the static, low-temperature g values of the CuN_6 polyhedra. The molecular $g_\parallel$ value in the dynamic region can be easily deduced from the average $\bar{g}$ value

$$\bar{g} = {}^1/_3(\langle g_1^{ex} \rangle + \langle g_2^{ex} \rangle + \langle g_3^{ex} \rangle) = {}^1/_3(\langle g_\parallel \rangle + 2\langle g_\perp \rangle)$$
$$\langle g_\parallel \rangle = 3\bar{g} - 2\langle g_\perp \rangle \tag{5}$$

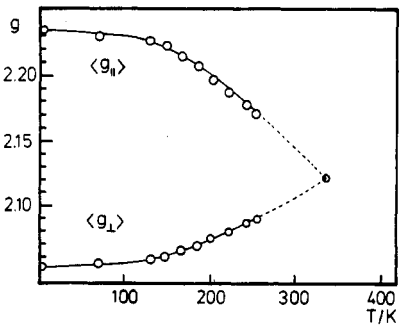

Figure 7. Temperature dependence of the molecular g values of $[Cu([9]aneN_3)_2][Cu(CN)_3]\cdot 2H_2O$.

The described situation corresponds to the dynamic change of the long copper–ligand spacings between Cu–N1(6) and the two equivalent Cu–N2(4) and Cu–N3(5) directions. While $A = 1$ characterizes the static limit below $\simeq 120$ K, $A = B = {}^1/_3$ indicates complete dynamic averaging with six equal Cu–N bond lengths at about 340 K (see below). From $\langle g_3^{ex} \rangle$ at 278 K[33] a B value of $\simeq 0.22$ is estimated, which can be easily translated into the geometry of the CuN_6 polyhedron by utilizing the Cu–N spacings for the static limit (110 K: $a_l = 2.32$ Å (2×), $a_s = 2.06$ Å (4×)) and the following equations in analogy to the expressions in eq 4:

$$\langle a_l \rangle = a_l - 2B(a_l - a_s) \qquad \langle a_s \rangle = a_s + B(a_l - a_s) \tag{6}$$

One obtains the partly dynamically averaged Cu–N bond lengths $\langle a_l \rangle = 2.21$ Å and $\langle a_s \rangle = 2.11_5$ Å, in close agreement with the structural data at 298 K (2.22 and 2.11 Å). The temperature dependence of $\langle g_\parallel \rangle$ and $\langle g_\perp \rangle$ is plotted in Figure 7. The extrapolation to $\langle g_\parallel \rangle = \langle g_\perp \rangle = \bar{g}$ leads to a temperature $T_c \simeq 340$ K, where the Cu–N bond lengths undergo complete dynamical averaging (compare also Figure 5). Consistent results with those of Figure 7 can be deduced from $\langle g_1^{ex} \rangle$ and $\langle g_2^{ex} \rangle$, but will not be given here.

The coefficients A and B in eq 4 and 6 can be interpreted as Boltzmann occupation factors, if one refers to the "Mexican hat" potential surface of octahedral Cu^{2+} with three minima, which results from the linear and nonlinear vibronic coupling of the electronic ^2E_g ground state with the vibrational ϵ mode.[28] We may assume that one of the three minima, which correspond to the three possible orientations of the long Cu–N bonds, is slightly stabilized by lattice forces with respect to the other two (energy difference ΔE). The thermal occupation of the two equivalent higher wells is then governed by a Boltzmann distribution.

The probability factor B is equal to

$$\frac{e^{-\Delta E/kT}}{1 + 2e^{-\Delta E/kT}}$$

in this model, and one obtains from eq 4 and 6 the following equation:

$$e^{-\Delta E/kT} = \frac{\delta g - \langle \delta g \rangle}{\delta g + 2\langle \delta g \rangle} = \frac{\delta a - \langle \delta a \rangle}{\delta a + 2\langle \delta a \rangle} \tag{7}$$

δg and δa are the differences between the molecular g values $g_\parallel$ and $g_\perp$ and between the long and short Cu–N spacings, respectively, in the static limit; $\langle \delta g \rangle$ and $\langle \delta a \rangle$ are the corresponding values in the (partially) dynamic region. Plots of calculated $\langle \delta g \rangle$ values vs. temperature—utilizing eq 7 with $\Delta E = 200$, 300, and 450 cm^{-1}—in comparison with the experimental $\langle \delta g \rangle$ values

(30) Abragam, A.; Bleaney, B. In *Electron Paramagnetic Resonance of Transition Ions*; Clarendon: Oxford, England, 1970; p 509.
(31) Reinen, D.; Dance, J. M. In *Inorganic Solid Fluorides*; Hagenmuller, P., Ed.; Academic: New York, 1985.
(32) Ozarowski, A.; Reinen, D. *Inorg. Chem.* **1985**, *24*, 3860.

(33) The single-crystal and powder EPR signals become too broad above 280 K in order to yield reliable g values.

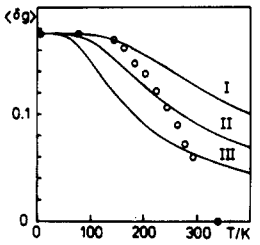

Figure 8. Temperature dependence of experimental and calculated $\langle \delta g \rangle$ values (eq 6), with ΔE = 200, 300, and 450 cm^{-1} (see text).

(Figure 8) clearly demonstrate that the applied model is only a very crude approximation. A more sophisticated theory would have to take into account explicitly the vibronic levels within the ground-state potential surface[34] and the fast relaxation between them, which leads to an averaging of the molecular g values and the Cu-N bond lengths at much lower temperatures than predicted by our simple model. Independent of a specific model, however, eq 4 and 6 allow us to correlate the extent of the Jahn-Teller distortion with the observed g values:

$$\frac{\langle \delta a \rangle}{\delta a} = \frac{\langle \delta g \rangle}{\delta g} \tag{8}$$

Thus the EPR investigations in dependence on temperature gave valuable information about the dynamic averaging process within the CuN_6 polyhedra, though complications due to exchange coupling effects occurred, and extended the results of the X-ray determinations at 298 and 110 K. Bonding parameters for the overlap between the metal $d_{x^2-y^2}$ orbital and the corresponding nitrogen s and p orbitals were also reported.

Acknowledgment. We thank the Fonds der Chemischen Industrie and the Deutsche Forschungsgemeinschaft for financial support. We thank Professor W. J. A. Maaskant (State University of Leiden) for helpful discussions. J.W. thanks the Netherlands Organisation for the Advancement of Pure Research (ZWO) for financial support.

Registry No. $[Cu([9]aneN_3)_2][Cu(CN)_3]\cdot 2H_2O$, 102920-57-0.

Supplementary Material Available: Tables of atom positional and anisotropic thermal parameters, bond distances and angles, and intraligand distances at 110 and 293 K (9 pages). Ordering information is given on any current masthead page.

(34) Riley, M. J.; Hitchman, M. A.; Reinen, D. *J. Chem. Phys.*, in press.

Contribution from the Departments of Chemistry and Physics, Faculty of Science, Kyushu University, Hakozaki, Higashiku, Fukuoka 812, Japan

Crystal Structure, Mössbauer Spectra, and Magnetic Properties of $[Fe(acpa)_2]PF_6$ and Crystallographic Changes in Fast Electronic Relaxation between $S = {}^1/_2$ and $S = {}^5/_2$

Yonezo Maeda,*† Hiroki Oshio,†§ Yoshimasa Takashima,† Masahiro Mikuriya,† and Masanori Hidaka‡

Received October 28, 1985

The crystal structure of the iron(III) complex $[Fe(acpa)_2]PF_6$ (Hacpa = *N*-(1-acetyl-2-propylidene)(2-pyridylmethyl)amine), which shows fast electronic relaxation between $S = {}^1/_2$ ($^2T_{2g}$) and $S = {}^5/_2$ ($^6A_{1g}$) with a spin-interconversion rate of about (2-3) × 10^6 s^{-1}, was determined. The crystal data for high-spin $[Fe(acpa)_2]PF_6$ ($FePF_6O_2N_4C_{22}H_{26}$) are as follows: monoclinic system, space group $P2/a$, a = 13.674 (1) Å, b = 9.911 (1) Å, c = 10.325 (1) Å, α = 90.00°, β = 110.43 (1)°, γ = 90.00°, V = 1311.3 (0) $Å^3$, R_w = 5.85%, d_{calcd} = 1.472, d_{found} = 1.46, Z = 2. The average bond distances, Fe-N = 2.117 Å and Fe-O = 1.939 Å, are in good agreement with the corresponding values reported for high-spin isomers of other spin-crossover iron(III) complexes. The temperature profiles of the integral intensities of (0n0) reflections derived from energy-dispersive X-ray diffraction were observed in the vicinity of the spin-transition temperature and showed a continuous variation with temperature which parallels that of the high-spin fraction. The results are interpreted in terms of a model in which the spin interconversions are accompanied by continuous atomic displacements within the same lattice and treated as an intramolecular mechanism.

Introduction

A number of spin-crossover iron complexes have so far been reported.[1-5] Recently iron(III) compounds that flip spin at a rate faster than the ^{57}Fe Mössbauer lifetime (1×10^{-7} s) have been reported.[6-11] A smooth increase of magnetic moments with increasing temperature is observed for complexes of this type, and those Mössbauer spectra show relaxation phenomena in the transition region. The magnetic property of the spin-crossover complex $[Fe(acpa)_2]PF_6$, which shows a spin-interconversion rate as fast as the Mössbauer lifetime of the excited state of ^{57}Fe, has been reported very recently.[6]

In the present experiment, energy-dispersive X-ray diffraction (EDD) was carried out to study structural transitions and/or the microstructural changes in the vicinity of a spin transition for this complex. It is important to observe a wide region of the wave vector Q (=$(4\pi \sin\theta)/\lambda$) to obtain microstructural information. The EDD method may be correlated to the usual angular-dispersive X-ray diffraction (ADD) by the following relations. In the EDD method, the Bragg condition is $2d_j \sin\theta = \lambda_j = 12.4/E_j$ (E in keV), on the other hand, $2d_j \sin\theta_j = \lambda$ in the ADD method. In the EDD method, experiments are done at fixed scattering angles and variable energy. The easy change in energy, E_j, is useful for selecting the energy of reflection outside the absorption edge of the constituent atoms in the specimen used. The EDD method is characterized by observing more reliable reflection

† Department of Chemistry.
‡ Department of Physics.
§ Present address: Institute for Molecular Science, Okazaki, Aichi 444, Japan.

(1) Ewalt, A. H.; Martin, R. L.; Sinn, E.; White, A. H. *Inorg. Chem.* **1969**, *8*, 1837.
(2) König, E.; Ritter, G.; Irler, W.; Goodwin, H. A. *J. Am. Chem. Soc.* **1980**, *102*, 4681.
(3) Rickards, R.; Johnson, C. E.; Hill, H. A. O. *J. Chem. Phys.* **1968**, *48*, 5231.
(4) Epstein, L. M.; Straub, D. K. *Inorg. Chem.* **1969**, *8*, 784.
(5) Hoselton, M. A.; Wilson, L. J.; Drago, R. S. *J. Am. Chem. Soc.* **1975**, *97*, 1722.
(6) Maeda, Y.; Tsutsumi, N.; Takashima, Y. *Inorg. Chem.* **1984**, *23*, 2440.
(7) Ohshio, H.; Maeda, Y.; Takashima, Y. *Inorg. Chem.* **1983**, *22*, 2684.
(8) Federer, W. D.; Hendrickson, D. N. *Inorg. Chem.* **1984**, *23*, 3861, 3870.
(9) Kunze, K. R.; Perry, D. L.; Wilson, L. J. *Inorg. Chem.* **1977**, *16*, 594.
(10) Hall, G. R.; Hendrickson, D. N. *Inorg. Chem.* **1976**, *15*, 607.
(11) Timken, M. D.; Hendrickson, D. N.; Sinn, E. *Inorg. Chem.* **1985**, *24*, 3947.

0020-1669/86/1325-2958$01.50/0